Simultaneous analysis of the elastic scattering and breakup channel for the reaction ^{11}Li + ^{208}Pb at energies near the Coulomb barrier

J. P. Fernández-García,[1,2,3,*] M. Cubero,[4,5] L. Acosta,[3,6] M. Alcorta,[7] M. A. G. Alvarez,[8] M. J. G. Borge,[4] L. Buchmann,[7] C. A. Diget,[9] H. A. Falou,[10] B. Fulton,[9] H. O. U. Fynbo,[11] D. Galaviz,[12] J. Gómez-Camacho,[1,2] R. Kanungo,[10] J. A. Lay,[1,13] M. Madurga,[4] I. Martel,[14] A. M. Moro,[1] I. Mukha,[15] T. Nilsson,[16] M. Rodríguez-Gallardo,[1] A. M. Sánchez-Benítez,[14,12] A. Shotter,[17] O. Tengblad,[4] and P. Walden[7]

[1]*Departamento FAMN, Universidad de Sevilla, Apartado 1065, 41080 Sevilla, Spain*
[2]*Centro Nacional de Aceleradores, Universidad de Sevilla, Junta de Andalucía-CSIC, 41092 Sevilla, Spain*
[3]*Istituto Nazionale di Fisica Nucleare - Laboratori Nazionali del Sud, INFN-LNS, I-95123 Catania, Italy*
[4]*Instituto de Estructura de la Materia, CSIC, Serrano 113 bis, 28006 Madrid, Spain*
[5]*Centro de Investigación en Ciencias Atómicas, Nucleares y Moleculares, CICANUM, CR-2060 San José, Costa Rica*
[6]*Instituto de Física, Universidad Nacional Autónoma de México, Apartado Postal 20-364, México D. F. 01000 México*
[7]*TRIUMF, V6T2A3 Vancouver, British Columbia, Canada*
[8]*Instituto de Física, Universidade de São Paulo, 05508-090 São Paulo, Brazil*
[9]*Department of Physics, University of York, YO-15DD Heslington, York, United Kingdom*
[10]*Department of Astronomy and Physics, Saint Mary's University, Halifax B3H3C3, Canada*
[11]*Department of Physics and Astronomy, Aarhus University, DK-8000 Aarhus, Denmark*
[12]*Centro de Física Nuclear da Universidade de Lisboa, CFNUL, 1649-003 Lisboa, Portugal*
[13]*Dipartimento di Fisica e Astronomia "Galileo Galilei", Università di Padova e INFN, Sezione di Padova, via Marzolo, 8, I-35131 Padova, Italy*
[14]*Departamento de Física Aplicada, Universidad de Huelva, E-21071 Huelva, Spain*
[15]*GSI, Helmholtzzentrum für Schwerionenforschung, G-64291 Darmstadt, Germany*
[16]*Fundamental Physics, Chalmers University of Technology, S-41296 Göteborg, Sweden*
[17]*School of Physics and Astronomy, University of Edinburgh, EH9 3JZ Edinburgh, United Kingdom*

(Received 24 July 2015; published 15 October 2015)

We present a detailed analysis of the elastic scattering and breakup channel for the reaction of ^{11}Li on ^{208}Pb at incident laboratory energies of 24.3 and 29.8 MeV, measured at the radioactive ion beam facility of TRIUMF, in Vancouver, Canada. A large yield of ^{9}Li fragments was detected by four charged particle telescopes in a wide angular range. The experimental angular and energy distributions of these ^{9}Li fragments have been compared to coupled-reaction-channel and continuum-discretized coupled-channel calculations. The large production of ^{9}Li fragments at small angles can be explained by considering a direct breakup mechanism, while at medium-large angles a competition between direct breakup and neutron transfer to the continuum of the ^{208}Pb target was observed.

DOI: 10.1103/PhysRevC.92.044608 PACS number(s): 25.70.−z, 24.50.+g, 25.60.−t

I. INTRODUCTION

The lithium isotope ^{11}Li has been one of the most studied nuclei. Setting the paradigm for halo nuclei, the ^{11}Li nucleus is characterized by a short half life (8.75(14) ms [1]), a very small two-neutron separation energy ($S_{2n} = 369.15(65)$ keV [2]) and a well-developed three-body structure, consisting of a ^{9}Li core and two loosely bound valence neutrons. It is also an archetype of Borromean system, since both the dineutron and the ^{10}Li system are unbound, whereas the three-body system is bound. Due to its loosely bound structure, the ^{11}Li nucleus exhibits a large $B(E1)$ strength at low excitation energies, characteristic of the neutron-halo nuclei. This property has been predicted by several theoretical models [3–7] and confirmed by Coulomb dissociation experiments [8–12].

As a consequence of the large low-lying $B(E1)$ strength, the ^{11}Li nucleus will be easily polarizable in the presence of a strong electric field. This occurs, for example, in collisions of ^{11}Li with a heavy target nucleus. At energies around and below the Coulomb barrier, where nuclear effects are expected to be small, this phenomenon, known as dipole Coulomb polarizability, produces a strong reduction of the elastic cross section with respect to the Rutherford prediction [13–16]. Moreover, the distortion of the projectile nucleus may lead to its dissociation, hence these experiments are usually accompanied by large breakup cross sections.

Recent advances in low-energy beam intensities in radioactive ion beam (RIB) facilities have allowed us to study these phenomena for several exotic nuclei, such as ^{6}He [14–19], ^{11}Be [20,21], and ^{11}Li [22,23] (see also Ref. [24] and references therein). This was the aim of the experiment performed at the TRI-University Meson Facility (TRIUMF) for the ^{11}Li+ ^{208}Pb reaction at energies around (29.8 MeV) and below (24.3 MeV) the Coulomb barrier ($V_B \approx 28$ MeV) [22,23]. As expected, the experiment showed a strong reduction of the elastic cross section with respect to the Rutherford formula and a large yield of ^{9}Li fragments. The observed deviation of

*fernandez@lns.infn.it

the elastic scattering with respect to the Rutherford formula was even larger than that expected from predictions based on a pure Coulomb dipole polarizability mechanism [25]. Since the neutrons were not detected in the experiment, the large yield of ^{9}Li could come from the ^{11}Li excitation to its continuum states, neutron transfer to the target nucleus, or even incomplete fusion.

In Refs. [22,23], the elastic and breakup data were compared with four-body continuum-discretized coupled-channel (4b-CDCC) calculations, using a three-body model of the ^{11}Li nucleus. These calculations provided a good agreement with both observables and confirmed that the large yield of ^{9}Li could be accounted for by considering a direct breakup mechanism, arising mainly from the strong dipole Coulomb couplings to the continuum states of ^{11}Li. The effect can be traced back to a large low-lying $B(E1)$ strength of the ^{11}Li nucleus. Moreover, the three-body model of ^{11}Li used in these CDCC calculations predicts the existence of a low-lying dipole resonance, which has been recently observed in Ref. [26]. In order to correctly reproduce the magnitude of the experimental breakup cross sections, this resonance needed to be placed very close to the threshold [23].

In this work, we present a more detailed analysis of the data. In addition to the angular distributions, the energy distributions of the ^{9}Li fragments at the two measured incident energies have been extracted and compared with several theoretical approaches. Since the calculation of this observable within the 4b-CDCC framework is not yet feasible, we have used the simpler 3b-CDCC approach, in which the ^{11}Li states are treated within a two-cluster (dineutron) model (^{9}Li $+2n$). Although this model can be questionable for a Borromean nucleus, such as ^{11}Li, we show that a proper choice of the dineutron model Hamiltonian provides elastic and breakup cross sections consistent with the more sophisticated 4b-CDCC calculations and hence with the measured data. However, although these 3b-CDCC calculations give a reasonable account of the angular and energy distributions of the ^{9}Li residues for angles up to $\sim 60^{\circ}$, at larger angles some underestimation of the data is observed. At these angles, nevertheless, the direct breakup mechanism assumed in the CDCC formalism might break down and other mechanisms might take place, such as transfer or inelastic breakup. The importance of these others mechanisms has been estimated by means of transfer to the continuum calculations. In these calculations, we consider the leak of flux of the elastic channel due to the coupling to one- and two-neutron transfer channels, leading to bound and unbound states of the ^{208}Pb $+1n$ and ^{208}Pb $+2n$ systems, respectively. These channels are coupled to the elastic channel to several orders (that is, beyond the Born approximation) thus performing a coupled-reaction-channel (CRC) calculation. Note that the transfer to ^{209}Pb and ^{210}Pb unbound states correspond also to breakup, but in a different basis representation, i.e., transferred neutron(s) relative to the target nucleus. The one- or two-neutron transfer representation will be more adequate to describe final states in which the neutrons are left with a small energy and angular momentum with respect to the target nucleus. These situations are expected to be more relevant at large scattering angles. On the other hand, the projectile representation (assumed in the CDCC formalism), will be more adequate for breakup configurations in which the energy in the relative motion of the ^{9}Li $+2n$ system is small. These configurations, with small energy transfer from the relative motion to the internal states, should dominate at forward scattering angles. The ^{9}Li production cross sections obtained in the transfer to the continuum calculations turn out to be small at small angles, but give sizable contributions at larger angles, supporting the idea that other mechanisms, rather than the direct breakup, take place at these angles.

The paper is organized as follows: first, we present the experimental setup and the measured energy spectra. Then, we present the elastic scattering of ^{11}Li+ ^{208}Pb reaction, at two different energies, as well as the angular and energy distributions of ^{9}Li fragments. We compare these data with theoretical calculations performed within the one-neutron transfer, two-neutron transfer to the continuum and direct breakup framework, using CRC and 3b-CDCC calculations, respectively. Finally in Sec. IV, we discuss and summarize the obtained results.

II. EXPERIMENTAL SETUP AND DATA

The experimental setup and analysis method were recently published in Refs. [22,23,27]. A summary is presented here.

The experiment was carried out using a postaccelerated ^{11}Li beam from ISAC-II at the TRIUMF facility at Vancouver, Canada. The ion beam was produced by a 500 MeV 100 μA proton beam, coming from the cyclotron, impinging on a Ta primary target. A pure ^{11}Li beam was obtained after the magnetic separator and postaccelerated by a SC-LINAC accelerator and delivered to the experimental setup, Fig. 1, in the ISAC-II hall.

The ^{11}Li beam was accelerated to laboratory energies of 24.3 and 29.8 MeV, with an average intensity around 4300 ions of ^{11}Li per second. Also a ^{9}Li beam was extracted and accelerated to the same center of mass energies in order to compare its behavior with that of ^{11}Li in reactions with the same target. In this way, we aimed to extract the effect of the two weakly bound halo neutrons in the dynamics of the reaction. In addition, stable ^{18}O^{+2} and ^{22}Ne^{+2} beams were used to optimize the transmission through the beam line of the ^{9}Li^{+1} and ^{11}Li^{+1} beams, respectively. A ^{208}Pb target was

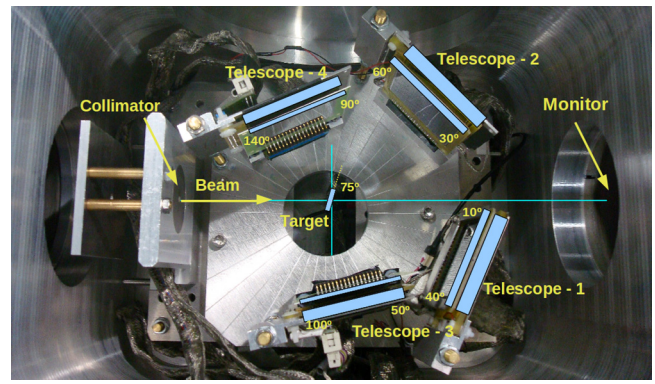

FIG. 1. (Color online) Picture of the experimental setup, where the different elements and telescope angular ranges are indicated.

TABLE I. Main characteristics of the experimental setup.

Telescope	Detec.	Thickness (μm)	Channels	Ang. range
T1	DSSSD	40	32	10°–40°
	PAD	500	1	10°–40°
T2	DSSSD	42	32	30°–60°
	PAD	500	1	30°–60°
T3	SSSSD	20	16	50°–100°
	DSSSD	63	32	50°–100°
T4	SSSSD	20	16	90°–140°
	DSSSD	63	32	90°–140°
Monitor	SBD	700	1	0°

placed at 75° with respect to the beam direction. We used a Pb target due to the stability of the double magic nucleus ^{208}Pb, which diminishes the contribution from excitations of the target. Two different target thicknesses of 1.45 mg/cm^2 and 1.9 mg/cm^2 were used for the study of the ^{9}Li+ ^{208}Pb reaction. As the production of ^{11}Li was acceptable and, in order to have the best energy resolution, only the thinner target of 1.45 mg/cm^2 was used for the study of the ^{11}Li+ ^{208}Pb reaction. A 5 mm diameter bismuth collimator was positioned at the entrance of the reaction chamber and a 700 μm surface barrier silicon detector (SBD) was placed approximately 28 cm downstream the target, as listed in Table I.

The setup was designed to cover an angular range from 10°–140° and to separate in mass and charge the different fragments coming from the ^{11}Li+ ^{208}Pb reaction. It consisted of four telescope systems. Forward angles (10°–60°) were covered by two telescopes consisting of a 40 μm thick double side silicon strip detector (DSSSD) of 16 × 16 strips, used to measure the energy loss (ΔE) of the reaction products (ΔE detector), and a 500 μm thick PAD, used to measure the remaining energy (E) of such products (E detector).

Each coincidence between a P- and a N-side strip of the DSSSD defines a detection pixel, which, coupled to the 500 μm PAD detector, results in a pixel telescope, which gives us the (ΔE, E) information of each event (reaction product), at forward angles, in the corresponding fired pixel. On the other hand, at medium-backward angles (50°–140°), two 20 μm single side silicon strip detector (SSSSD) of 16 strips were used to measure the energy loss (ΔE) of the reaction products and coupled to two 60 μm DSSSD's, which were used to measure the remaining energy (E) of the products. Again, each coincidence between a P- and a N-side strip, now of a 60 μm DSSSD, defines a detection pixel, which, coupled to the thin 20 μm SSSSD results on a pixel telescope, that gives us the (ΔE, E) information of each event, at medium-backward angles, in the corresponding fired pixel.

In Table I, the main characteristics of the experimental setup are summarized. A schematic view of the experimental setup is shown in Fig. 1. More details can be found in Ref. [27].

The energy calibration was performed using triple α (^{239}Pu - ^{241}Am - ^{244}Cm) and ^{148}Gd sources. To obtain the energy calibration, the energy losses in the different dead layers of the detectors were calculated using the stopping and range tables of the Stopping Range of Ions in Matter (SRIM) package [28] and incorporated in the energy calibration procedure.

In order to normalize the response of the four telescope systems, the elastic scattering angular distribution of the ^{9}Li+ ^{208}Pb reaction at a laboratory incident energy of 24.03 MeV was measured. At such energy, the Rutherford behavior, $1/\sin^4(\theta_{\rm c.m.}/2)$, should be expected for the full angular range. The solid angle was calculated for each pixel of each detector based on its distance to the target and laboratory angles.

The bidimensional spectra, ΔE versus total energy, $\Delta E + E$, obtained with the telescope systems T1 and T2 for the two different ^{11}Li beam energies are shown in Fig. 2. Using the pixel energy calibrations, we are able to determine the energy distribution of the breakup products as well as to separate them from the elastic ones, as shown in Fig. 2.

Due to the clear separation between the elastic (^{11}Li) and breakup (^{9}Li) events in the telescopes T1 and T2, we could choose the same selection region in the bidimensional plot to identify the elastic scattering and breakup events, displayed with solid red and dashed blue lines, respectively. This procedure was not used for the telescope systems T3 and T4 because the elastic and breakup process were not well separated in these telescopes. In such case, the pixels of each telescope were integrated in angular bins of 3°, which allows us to define the different integration areas. In Fig. 3, the bidimensional diagrams for the telescope T3 and T4 considering the angular bin of 58.0(1.5)° and 130.0(1.5)°, respectively, are represented.

After the energy calibration of each pixel, the number of breakup counts were binned in energy intervals of 500 keV. To obtain reasonable statistics, all pixels in the angular intervals of 10°–30°,30°–50°,50°–90°, and 90°–140° were added together. Then, using the solid angles and the average beam intensity of 4300 ^{11}Li/s over the time of the measurement, the breakup cross sections were obtained.

The experimental elastic scattering angular distributions are shown in Figs. 4 and 5 by the data points and compared to several calculations discussed in Sec. III. They show a remarkable suppression of the ^{11}Li elastic cross section with respect to the Rutherford formula [22], even at very forward angles. Note that data oscillations around 75°–90° could be due to systematic uncertainties associated with the target shadow in detector 3, as shown in Fig. 1. These data should be treated with caution. To study the role of the breakup channel, the angular and energy distributions of the ^{9}Li fragments are represented in Figs. 6 and 7, respectively. These observables have been compared to 3b- and 4b-CDCC and CRC calculations, as described, in detail, in Sec. III.

III. THEORETICAL CALCULATIONS

In this section, we compare the elastic scattering and breakup experimental data with 3b-CDCC and CRC calculations. The first one is based on a direct breakup (DBU) model, in which the breakup process is treated as an inelastic excitation of the projectile. CRC calculations assume a two-neutron or one-neutron transfer mechanism populating bound and unbound states of the 2n-target or 1n-target systems (2n-TC

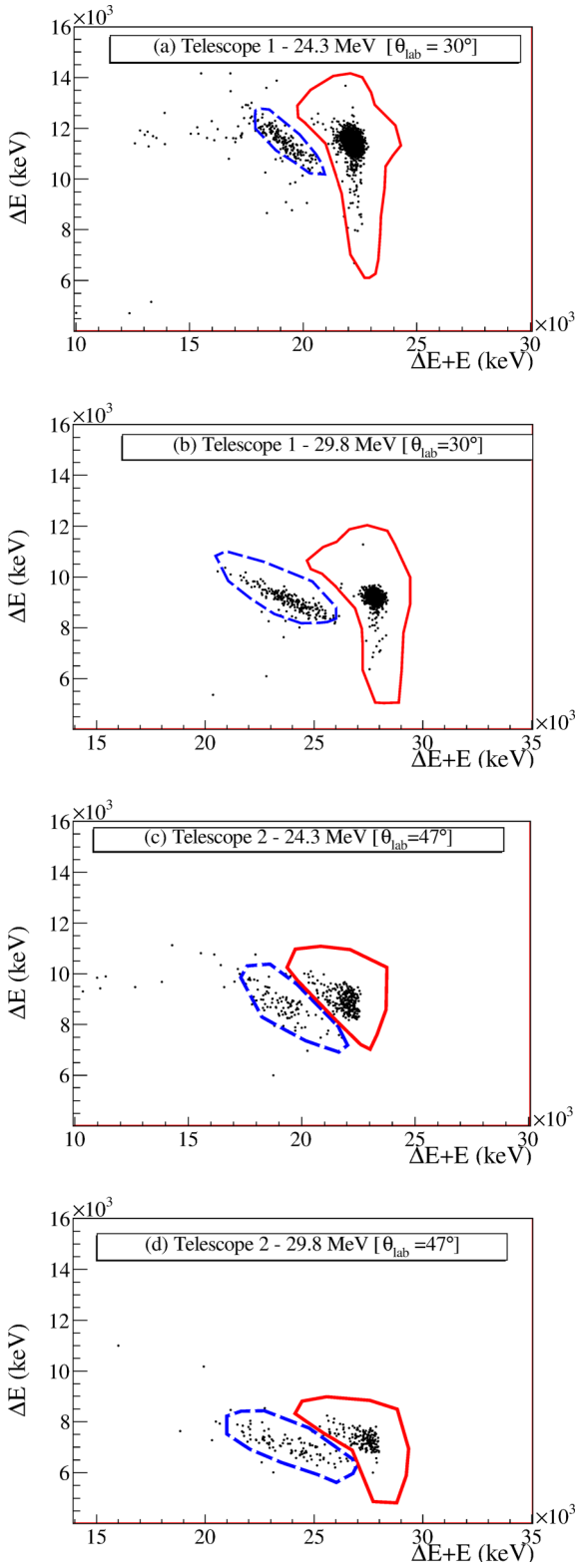

FIG. 2. (Color online) Experimental bidimensional diagrams for the telescopes 1 [(a) and (b)] and 2 [(c) and (d)] at two different incident energies (24.3 and 29.8 MeV), integrated for the pixels corresponding to the angular bins of 30.0(1.5)° and 47.0(1.5)°, respectively. The different selection windows used for the elastic and breakup events are displayed by solid red and dashed blue lines, respectively.

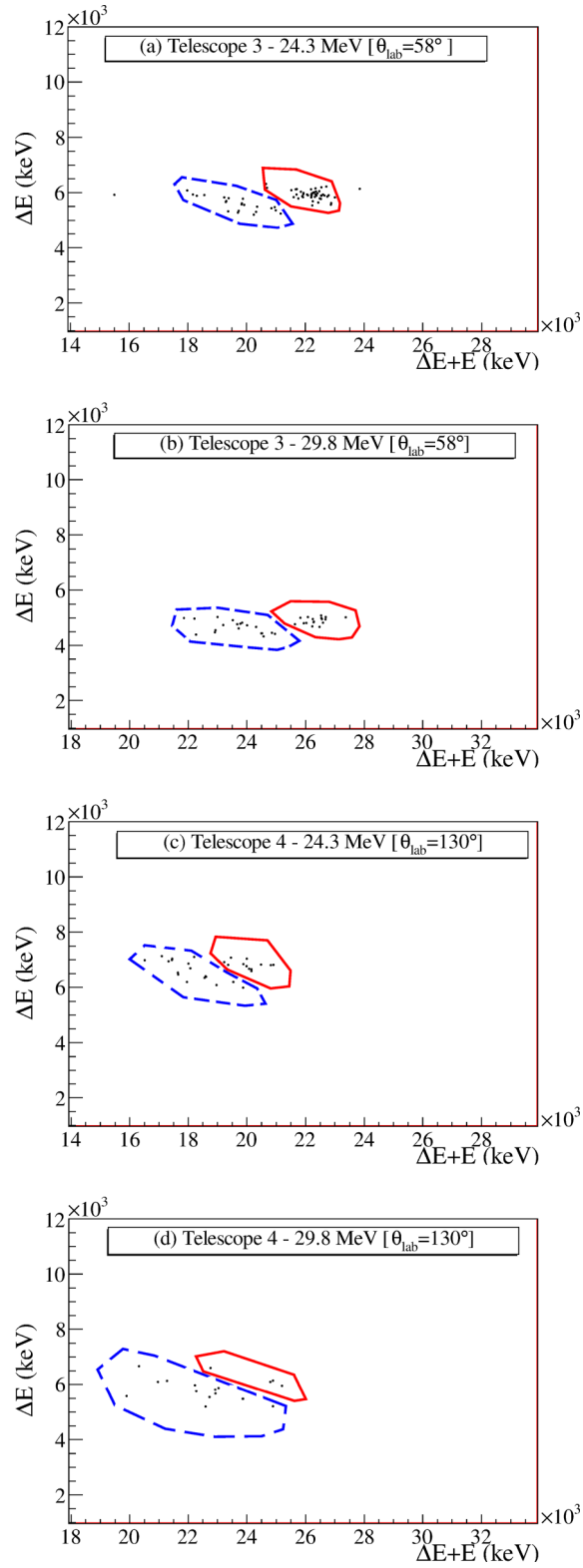

FIG. 3. (Color online) Experimental bidimensional diagrams for the telescopes 3 [(a) and (b)] and 4 [(c) and (d)] at two different incident energies (24.3 and 29.8 MeV), integrated for the pixels corresponding to the angular bins of 58.0(1.5)° and 130.0(1.5)°, respectively. The different selection windows used for the elastic and breakup events are delimited by solid red and dashed blue lines, respectively.

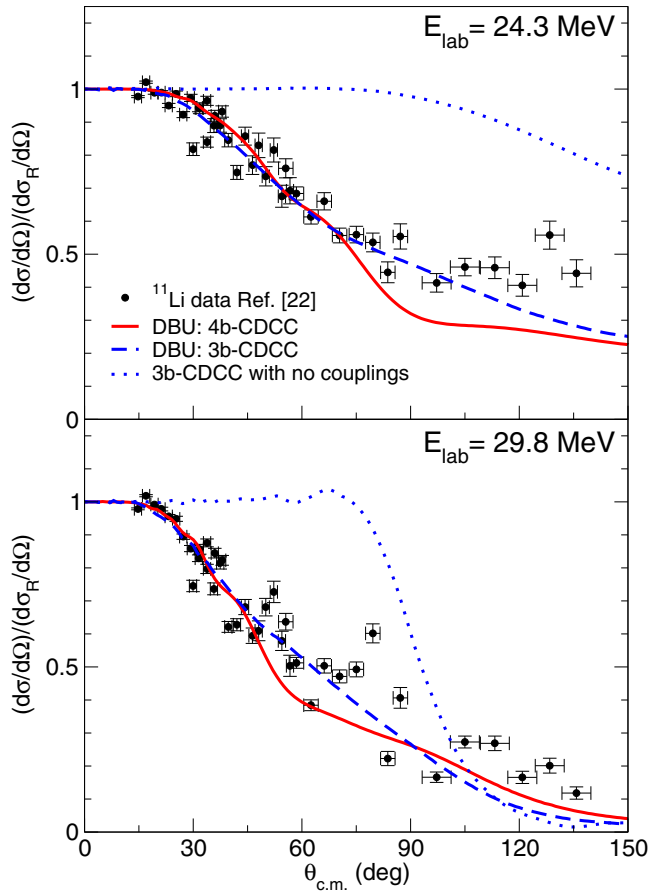

FIG. 4. (Color online) Elastic scattering angular distributions, in the center-of-mass frame, at two different bombarding energies. The 4b- and 3b-CDCC calculations are represented by solid red and dashed blue lines, respectively. The same 3b-CDCC calculations without the continuum couplings are shown by dotted blue lines.

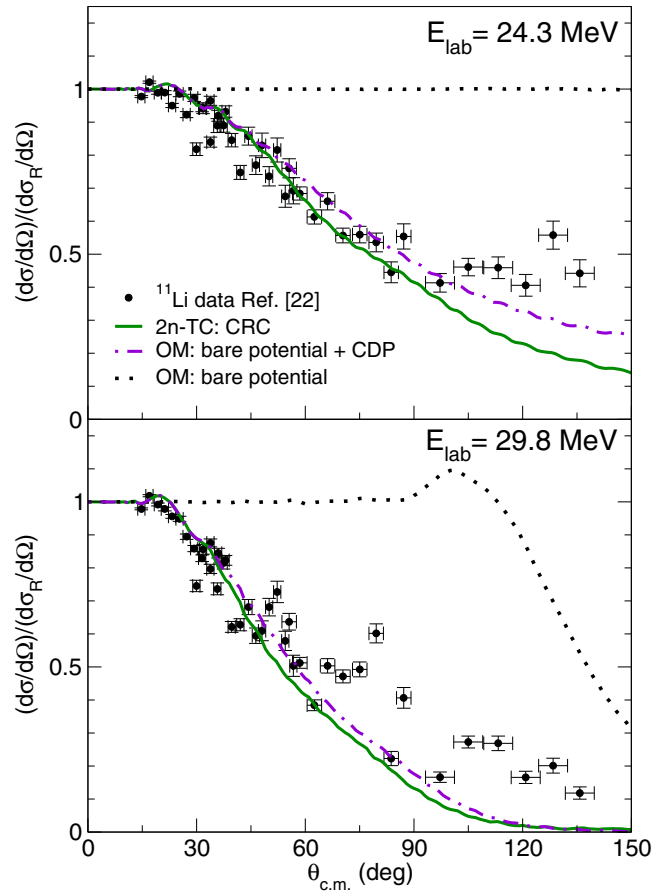

FIG. 5. (Color online) Elastic scattering angular distributions, in the center-of-mass frame, at two different bombarding energies. The dotted line is the one-channel (no-continuum) calculation using the double-folding SPP potential. The dot-dashed line is the one-channel calculation with the SPP potential plus the Coulomb dipole polarization potential (CDP). The solid lines are the full CRC calculations.

and 1n-TC model). The aim of this study is to understand the dynamics of the reaction induced by the weakly bound nucleus, ^{11}Li, on a heavy target.

In order to obtain a first understanding of the breakup process, we compare the experimental energy distributions of the ^{9}Li fragments with two limits derived from simple kinematic considerations for the DBU and 2n-TC models. In the first one, the ^{11}Li nucleus is slightly excited by the target. In this case, we would expect the velocity of the outgoing ^{9}Li ejectiles to be similar to that of the elastic scattered ^{11}Li. Therefore, its energy would be a 9/11 fraction of the incident ^{11}Li energy. On the other hand, the 2n-TC picture considers a reaction mechanism in which the two neutrons loose part of their kinetic energy and are left with small relative energy with respect to the target. Hence, the ^{9}Li particles remain with essentially the beam energy.

In Fig. 7, the predicted energy of the DBU and 2n-TC mechanisms are represented by the solid blue and dashed green arrows, respectively. The comparison of these two extreme models with the experimental data suggests a dominance of the DBU mechanism at forward angles (telescopes 1 and 2), while for large angles (telescopes 3 and 4) both extreme models give energies compatible with the data.

From the same figure it is seen that, for the smallest scattering angles, the average energy of the emitted ^{9}Li products is close to 9/11 that of the incoming ^{11}Li. However, as the scattering angle increases, the average energy of ^{9}Li is larger than this simple expectation by ∼1–2 MeV, meaning that they are postaccelerated. This energy gain can be understood as a postacceleration of the ^{9}Li fragments due to the Coulomb potential, following the breakup of the projectile in the proximity of the target. For example, for a scattering angle of 40° and at 29.8 MeV, the energy gain in a classical Coulomb trajectory is around 2 MeV, in agreement with Fig. 7.

For a more quantitative understanding of the data, we have compared the angular and energy distributions of the ^{9}Li breakup fragments with the predictions of the 3b-CDCC and CRC calculations described in the following sections.

A. Direct breakup mechanism (CDCC calculations)

The CDCC framework [29,30] has been successfully used to describe reactions using either a three-body (two-body

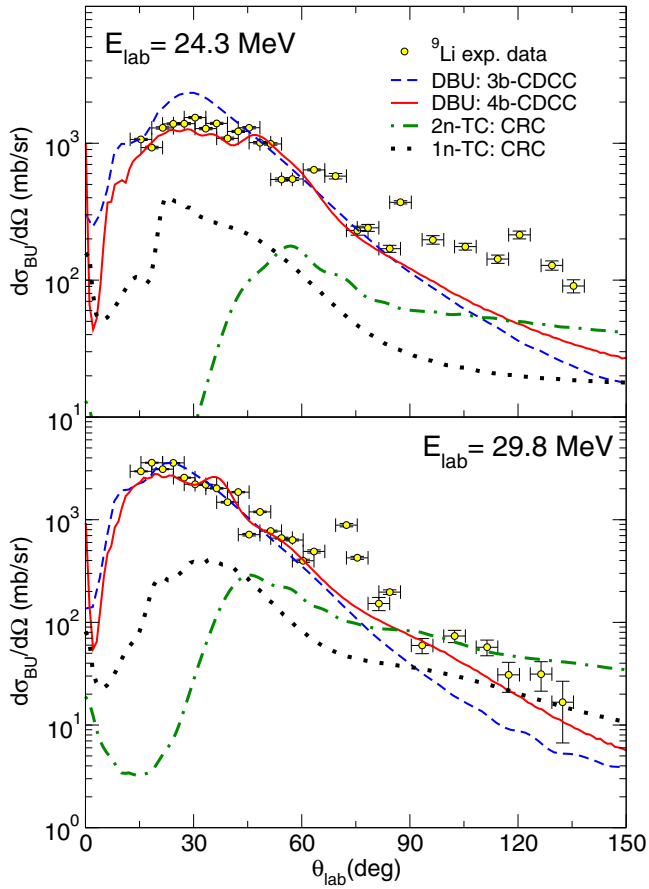

FIG. 6. (Color online) Angular distributions of the ^{9}Li fragments, in the laboratory frame, for the reaction ^{11}Li+ ^{208}Pb at incident energies of 24.3 and 29.8 MeV. The solid red and dashed blue lines are the 4b- and 3b-CDCC calculations, while the CRC calculations assuming a two- or one-neutron transfer mechanism are represented by dot-dashed green and dotted black lines, respectively.

projectile + target) or a four-body model (three-body projectile + target) reaction model [31–37].

Due to the difficulties of calculating the energy and angular distributions of the breakup fragments in a four-body reaction model, first we consider the collision as a three-body problem, which is based on a two-body model of ^{11}Li (^{9}Li+2n). We use the dineutron, 2n, model similar to that proposed in Ref. [13] for the ^{6}He nucleus, where the relative motion between the two valence neutrons is ignored and only the 2n-core degree of freedom is taken into account. Furthermore, in the dineutron model, the two valence neutrons are assumed to be coupled to spin zero and bound to an inert ^{9}Li-core. The binding potential of Ref. [38] was used for the ^{9}Li-2n interaction, consisting of a Woods-Saxon parametrization with radius $R_0 = 2.270$ fm and diffuseness parameter $a_0 = 0.20$ fm. This model uses an adjusted depth in order to reproduce the experimental two-neutron separation energy, $S_{2n} = 369.15(65)$ keV [2].

For the ^{9}Li+ ^{208}Pb interaction, we consider the optical potential of Ref. [27], consisting of a double-folding São Paulo potential (SPP) [39] for the real part and a Woods-Saxon parametrization for the imaginary part, whose parameters were fitted to the ^{9}Li+ ^{208}Pb data obtained in the present experiment. As for the ^{208}Pb-2n interaction, it was calculated using the following single-folding model:

$$U(R) = \int \rho(\vec{r}_{nn}) \left[U_n\left(\vec{R} + \frac{\vec{r}_{nn}}{2}\right) + U_n\left(\vec{R} - \frac{\vec{r}_{nn}}{2}\right)\right] d\vec{r}_{nn},$$

where $\vec{R}$ is the coordinate ^{208}Pb-2n, U_n is the neutron-target optical potential [40] and $\rho(\vec{r}_{nn})$ is the density probability along the r_{nn} coordinate calculated within the ^{11}Li three-body model of Ref. [23]. Continuum states with relative angular momentum $\ell_i = 0$–6 and excitation energies up to 8 MeV above the breakup threshold were considered and discretized using the standard binning method. Both Coulomb and nuclear effects were included. These calculations were performed using the code FRESCO [41].

The calculated elastic scattering angular distributions are compared with the experimental data in Fig. 4. Despite the simplicity of this dineutron model for ^{11}Li, the experimental data are very well reproduced by such calculations and are in good agreement with the more realistic 4b-CDCC calculations of Ref. [23]. To assess the importance of coupling to the continuum states, in Fig. 4, we present also the calculations without such couplings (dotted lines). These calculations largely overestimate the experimental data for angles larger than 30° and, at $E = 29.8$ MeV, show a maximum of the elastic cross section, reminiscent of the Fresnel interference peak.

In Fig. 8, the $B(E1)$ distribution obtained with the three-body model of ^{11}Li of Ref. [23] and that obtained with the dineutron model of Ref. [38] are compared with the experimental $B(E1)$ extracted in Ref. [11] from the Coulomb dissociation data. At excitation energies close to the breakup threshold, both, dineutron and three-body models, suggest more $B(E1)$ strength than that extracted in Ref. [11]. The origin of this discrepancy is unclear to us and further theoretical and experimental work is called for in order to elucidate it.

We next analyze the angular and energy distributions of the ^{9}Li outgoing fragments. In Figs. 6 and 7, the calculated distributions are compared with the experimental data. For the DBU calculations, these observables were calculated applying the appropriate kinematic transformation to the scattering amplitudes obtained in the CDCC calculations, using the codes and the formalism developed in Refs. [35,42]. In the case of 4b-CDCC calculations, the angular distributions were calculated assuming the scattering angle of the center of mass (c.m.) of the ^{11}Li instead of the ^{9}Li scattering angle [23]. DBU calculations (3b- and 4b-CDCC) describe well the position of the maximum and the width of the ^{9}Li energy distributions at forward angles. This supports the idea that, at least at forward angles, DBU is the dominant mechanism.

Concerning the angular distributions, the 4b-CDCC calculations are seen to reproduce well the data up to about 60°, but underestimate them for larger angles. On the other hand, 3b-CDCC calculations give a qualitatively similar trend, but overestimate the magnitude by almost a factor of 2 at small angles. This is due to the limitation of the dineutron model, that, as it can be seen in Fig. 8, overpredicts the $B(E1)$ distributions at low excitation energies.

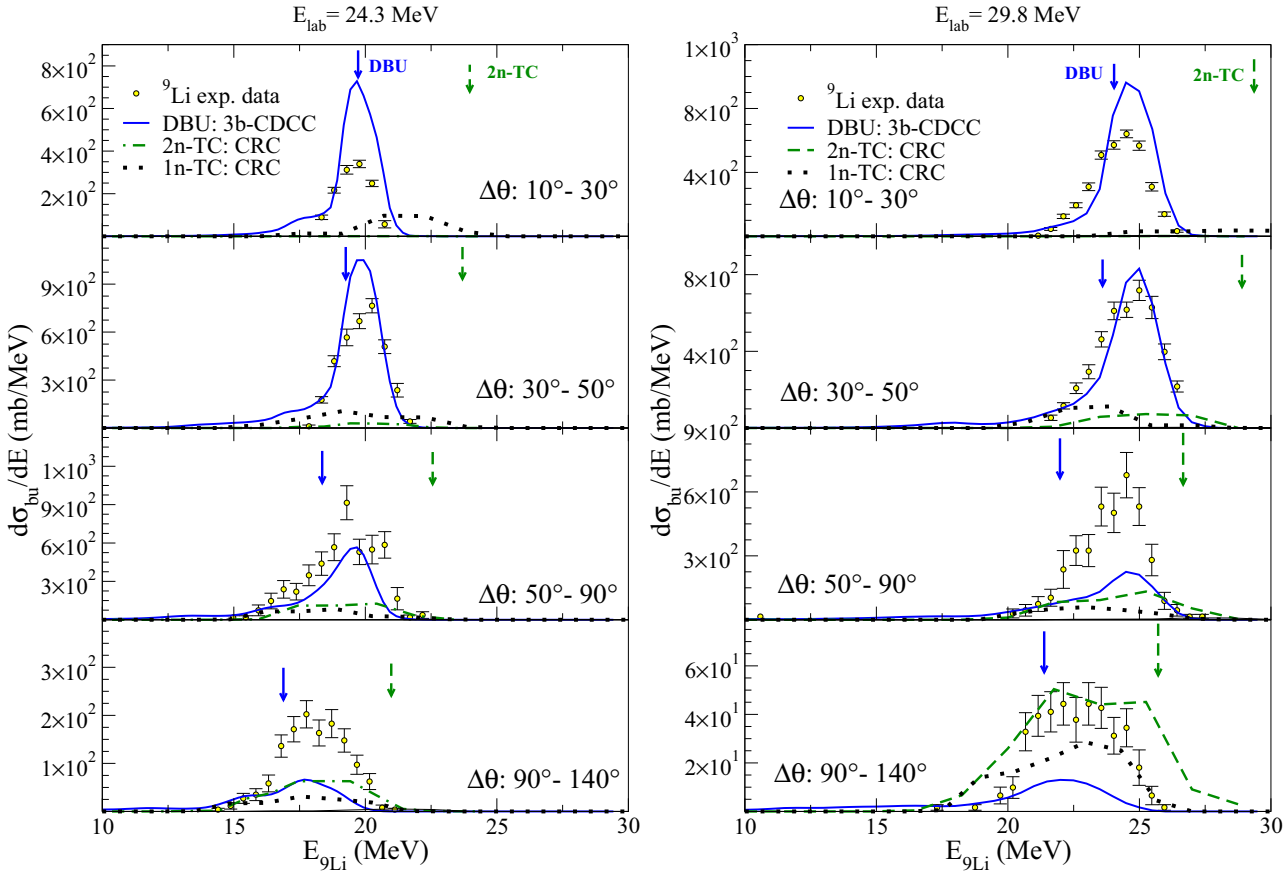

FIG. 7. (Color online) Energy distributions of the outgoing ^{9}Li fragments from the reaction ^{11}Li+ ^{208}Pb at the laboratory incident energies of 24.3 (left) and 29.8 (right) MeV for four angular ranges covering angles from 10°–140°. 3b-CDCC calculations are represented by solid blue lines. Blue solid and dashed green arrows typify the energy expected by the DBU and 2n-TC mechanisms. The dashed green and dotted black lines are the CRC calculations assuming a two- or one-neutron transfer mechanism, respectively.

B. Two-neutron transfer mechanism (CRC calculations)

In the CRC formalism, we consider an alternative model to describe the two-neutron removal process. The model assumes a two-neutron transfer mechanism, in which the two valence neutrons of the projectile are transferred to bound and unbound states of the 2n-target system. CRC calculations have been recently used to describe the reactions induced by ^{6}He, another Borromean nucleus, on ^{208}Pb [19], ^{64}Zn [43], and ^{120}Sn [44].

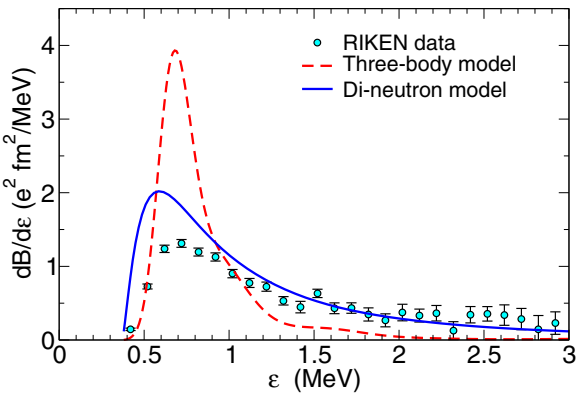

FIG. 8. (Color online) $B(E1)$ distributions of ^{11}Li as a function of the excitation energy. The circles represent the experimental distribution extracted in Ref. [11]. The dashed line corresponds to the three-body model calculation of ^{11}Li [23], while the solid line is the $B(E1)$ distributions obtained using the two-body model of ^{11}Li of Ref. [38].

In order to have a meaningful comparison between both formalisms, 3b-CDCC and CRC, we consider the same dineutron model for ^{11}Li and adopt the same potential for the ^{9}Li-2n, ^{208}Pb-2n, and ^{9}Li-^{208}Pb systems used in the 3b-CDCC calculations. For the ^{208}Pb-2n interaction, nevertheless, only the real part is considered in order to allow the inclusion of bound states. Moreover, it has been formally shown that this choice of the fragment-target interaction provides, in addition to the elastic breakup component, contributions from nonelastic breakup, that is, breakup accompanied by target excitation or neutron absorption [45]. We note that, by construction, this nonelastic breakup is absent in the CDCC calculations.

In the CRC calculations, the elastic scattering is modified by the coupling to the two-neutron transfer channels, populating bound and unbound states of the ^{208}Pb-2n system. To avoid double counting, a bare potential is considered for the ^{11}Li+ ^{208}Pb system. For that, in this work we have used the SPP double-folding potential, taking into account the Gaussian-oscillator and Fermi-Dirac distributions of Refs. [46]

and [39] for the ^{11}Li and ^{208}Pb matter densities, respectively. The SPP potential is supplemented with a Coulomb dipole polarization (CDP) potential, which includes, in an effective way, the effect of the Coulomb couplings of the projectile. Here, we use the semiclassical model proposed in Ref. [25], whose main ingredient is the $B(E1)$ distribution of the projectile. For that, we use the $B(E1)$ calculated with the three-body approach of ^{11}Li used in the 4b-CDCC calculations. The bare interaction includes also a short-range Woods-Saxon imaginary potential with parameters $W = 50$ MeV, $R = 8.15$ fm, $a_0 = 0.1$ fm, to simulate the ingoing boundary condition for fusion.

To construct the ^{210}Pb* final states, we follow the procedure described in Ref. [18], where the energy spectrum was described by a set of representative states for each value of the relative angular momentum of the ^{208}Pb-$2n$ system (ℓ_f). Above the two-neutron breakup threshold, these states were discretized using 2 MeV bins up to 8 MeV. For energies below the threshold, five bound states for each ℓ_f, spaced by 1 MeV, were considered. To obtain convergence of the observables, it was necessary to include partial waves up to $\ell_f = 8$ for the ^{208}Pb-$2n$ relative motion. These CRC calculations were also performed with the code FRESCO [41]. For a meaningful comparison with the data, the calculated cross sections were then transformed to the laboratory frame.

In Fig. 5, we compare these calculations with the elastic data. The full CRC calculations reproduce well the measured distributions, at both incident energies. We have included also two single-channel calculations. The dotted line is the calculation using the bare potential alone. At the lower energy, this calculation is very close to the Rutherford result, whereas at the higher energy, it exhibits a Fresnel-like pattern. In both cases, it departs significantly from the data. The dot-dashed line is a single-channel calculation including the bare + CDP potential. It is seen that the CDP produces a strong reduction of the elastic data for angles larger than 20°, and gives a result much closer to the data. Inclusion of the $2n$ transfer channels (solid line) has a small influence. This result confirms that the observed suppression of the elastic data is mostly due to the dipole Coulomb couplings, consistently with the CDCC results.

The calculated angular and energy distributions of the ^{9}Li particles are compared with the experimental data in Figs. 6 and 7, respectively. The CRC calculations underestimate the data at forward angles but give a more significant contribution at larger angles, where the DBU calculations start to underpredict the data. This result suggests that, at these large angles, the DBU model breaks down, and the transfer picture becomes more appropriate to describe the production of ^{9}Li. The underestimation at small angles can be attributed to the fact that the breakup events produced at these angles are mostly produced by the dipole Coulomb excitation. In our CRC scheme, in which the breakup states are described in terms of ^{208}Pb-$2n$ states, the explicit account of the breakup mechanism produced by the dipole Coulomb excitation would require the inclusion of very large values of ℓ_f. Note, however, that its effect on the elastic scattering is taken into account effectively through the CDP potential.

C. One-neutron transfer mechanism (CRC calculations)

Another channel that could contribute to the production of ^{9}Li particles is the one neutron transfer, ^{208}Pb(^{11}Li, ^{10}Li)^{209}Pb. Since the $s_{1/2}$ and $p_{1/2}$ states give the main contribution to the ^{11}Li ground state (g.s) wave function, with almost the same probability [6,47], these two configurations have been considered. In the $s_{1/2}$ configuration the ^{10}Li could be in the virtual state 1^- or 2^-, while in the $p_{1/2}$ it could be in the resonant state 1^+ or 2^+. This process will produce ^{10}Li, which will decay into ^{9}Li $+n$. The calculations for this process were performed within the CRC formalism. We included the known bound states for the ^{209}Pb nucleus, and assumed unit spectroscopic factors, since these are known to be mainly single-particle states.

In a simple mean-field picture of ^{11}Li, the two valence neutrons would have a pure $(s)^2$ or $(p)^2$ configuration. More elaborate models (see, e.g., [48–50]) as well as knockout experiments indicate that the g.s. of ^{11}Li consists of a mixture of $(s)^2$ and $(p)^2$ with similar proportion [51]. Moreover, some of these theoretical models indicate that a significant part of the wave function consist in excited components of the ^{9}Li-core, which are expected to lead to final states where ^{9}Li does not survive. Using the wave function of [48,49], and neglecting these excited-core components, one gets the spectroscopic factors $S(s_{1/2}) = 0.405$ and $S(p_{1/2}) = 0.605$. These values have been adopted for the present $1n$-transfer calculations

For the entrance channel, ^{11}Li + ^{208}Pb, the OM potential is the sum of the SPP and CDP potentials. For the exit channel, ^{10}Li + ^{209}Pb, the same potential ^{9}Li + ^{208}Pb used in the 3b-CDCC calculations was considered. The binding potential for ^{9}Li+n was taken from Ref. [38].

The calculated angular distributions are shown by the dotted black lines in Fig. 6. It should be noted that, in this case, the scattering angle corresponds to the center of mass of the ^{10}Li* system, rather than the ^{9}Li angle. At small angles ($\theta_{\rm lab} < 60°$), our calculations predict a significant contribution of the $1n$ transfer, although the ^{9}Li yield is still dominated by the DBU mechanism. It can also be seen that at large angles ($\theta_{\rm lab} > 60°$), the contribution of the $1n$ transfer to the production of ^{9}Li particles is comparable to that due to the $2n$ transfer. In Fig. 7, the calculated energy distributions can explain reasonably the energy of the ^{9}Li fragments, mainly at large angles. Note that, in this case, the maximum kinetic energy of the ^{9}Li particles emitted in one-neutron transfer process corresponds to a 9/10 fraction of the incident ^{11}Li energy, 21.9 and 26.8 MeV for low and high energies, respectively.

To conclude, in Table II, the experimental total reaction and the breakup cross sections are compared with those obtained from the different breakup mechanisms. The experimental total reaction cross sections were obtained from the OM fit of the elastic scattering data, while the experimental breakup cross sections are the integral over the energy (or ^{9}Li angle) of the experimental energy (or angular) distributions. These numbers may contain the yield of ^{9}Li fragments coming from all possible breakup processes, such as elastic breakup, nonelastic breakup, or neutron transfer.

TABLE II. Comparison of the experimental total reaction cross section ($\sigma_{\rm reac}$) and breakup cross section (σ_{BU}) with the DBU, $2n$-TC and $1n$-TC mechanisms. The experimental reaction cross sections are obtained from the optical model fit to the elastic differential cross sections (see text for details).

24.3 MeV	Exp. (mb)	DBU(4b-CDCC) (mb)	2n-TC (CRC) (mb)	1n-TC (CRC) (mb)
$\sigma_{\rm reac}$	5400	6500	5500	5600
σ_{BU}	5100	4200	780	940
29.8 MeV	Exp. (mb)	DBU(4b-CDCC) (mb)	2n-TC (CRC) (mb)	1n-TC (CRC) (mb)
$\sigma_{\rm reac}$	7800	8400	7100	7900
σ_{BU}	6500	5400	1100	1000

One can observe that the breakup process constitutes the main contribution to the reaction cross sections and that the direct breakup mechanism seems to be dominant.

IV. DISCUSSION AND SUMMARY

We have measured the elastic scattering differential cross sections and the angular and energy distributions of the ^{9}Li fragments arising from the inclusive breakup of the reaction ^{11}Li+ ^{208}Pb at two incident energies around and below the Coulomb barrier. We observed a strong reduction of the elastic cross sections, accompanied by a large yield of ^{9}Li.

We can reasonably describe the three observables, at small and intermediate angles ($\theta < 60^{\circ}$), with CDCC calculations, which describe the elastic scattering and the elastic breakup cross sections. For the latter, the main mechanism is dipole Coulomb breakup. This confirms the idea that elastic and inclusive breakup measurements, at energies around the Coulomb barrier, can be used as a tool to extract information on the $B(E1)$ distribution at these energies, but there should be an awareness that systematic analysis errors can arise if due account is not given to other mechanisms arising from nuclear interactions.

At larger scattering angles, beyond 60°, the CDCC calculations underestimate the experimental data. This indicates that other mechanisms for removing the neutrons from ^{11}Li play an important role, such as transfer to bound states of the target, or nonelastic breakup. These effects have been estimated using two different approaches:

(i) The CRC calculations assume a dineutron model for the ^{11}Li nucleus and include, in addition to the elastic channel, a set of representative states for the ^{208}Pb -2n systems, which are meant to simulate the two-neutron transfer and total breakup (elastic + inelastic). Since dipole Coulomb breakup is not expected to be well described by the two-neutron transfer representation, this effect is approximated by an analytical Coulomb polarization potential. These CRC calculations give important contributions at backward angles and predict the energy distributions of the ^{9}Li fragments, slightly shifted to higher energies, and consistent with the data.

(ii) The CRC calculations for one neutron transfer, describing ^{11}Li as a combination of s and p neutrons, coupled to ^{10}Li in 1^{+}, 2^{+} virtual states or 1^{-}, 2^{-} resonances. The calculations give sizable contributions at backward angles, which are comparable to those of the CRC calculations for two-neutron transfer.

It should be noted that these transfer calculations (i) and (ii), do not necessarily lead to orthogonal states, and are not, *a priori*, orthogonal to the direct breakup calculations. So, one should not attempt to add up the corresponding cross sections. Calculations (i) and (ii) only show that the reaction mechanism, at backward angles, is more complex than the pure direct breakup, and so it would be much more difficult to extract spectroscopic information from the cross sections at backward angles. We emphasize, however, that the breakup cross sections at these large angles are much smaller than those at smaller angles and, therefore, the direct breakup mechanism is able to account for most of the measured ^{9}Li cross sections.

To conclude, the observables measured in this work have demonstrated that the extremely weakly bound structure of ^{11}Li is easily broken, producing a large yield of ^{9}Li fragments. This effect is appropriately described by a direct breakup model, mainly at forward angles, although at backward angles other mechanisms, such as neutron transfer or nonelastic breakup, become important.

ACKNOWLEDGMENTS

This work has been partially supported by Spanish National Projects No. FPA2009-08848, No. FPA2009-07387, No. FPA2010-22131-C02-01, No. FPA2009-07653, No. FPA2012-32443 and by the Consolider-Ingenio 2010 Program CPAN (CSD2007-00042). M.R.G. acknowledges the financial support from the program VPPI-US. C.A.D acknowledges the financial support from the U.K. Science and Technology Facilities Council through Grant No. EP/D060575/1. J.A.L. acknowledges a Marie Curie Piscopia fellow at the University of Padova.

[1] J. H. Kelley, E. Kwan, J. E. Purcell, C. G. Sheu, and H. R. Weller, Nucl. Phys. A **880**, 88 (2012).

[2] M. Smith *et al.*, Phys. Rev. Lett. **101**, 202501 (2008).

[3] A. A. Korsheninnikov *et al.*, Phys. Rev. Lett. **78**, 2317 (1997).

[4] K. Ikeda, Nucl. Phys. A **538**, 355 (1992).

[5] E. Garrido, D. V. Fedorov, and A. S. Jensen, Nucl. Phys. A **708**, 277 (2002).
[6] T. Myo, K. Kato, H. Toki, and K. Ikeda, Phys. Rev. C **76**, 024305 (2007).
[7] Y. Kikuchi, T. Myo, K. Kato, and K. Ikeda, Phys. Rev. C **87**, 034606 (2013).
[8] K. Ieki *et al.*, Phys. Rev. Lett. **70**, 730 (1993).
[9] S. Shimoura, T. Nakamura, M. Ishihara, N. Inabe, T. Kobayashi, T. Kubo, R. H. Siemssen, I. Tanihata, and Y. Watanabe, Phys. Lett. B **348**, 29 (1995).
[10] M. Zinser *et al.*, Nucl. Phys. A **619**, 151 (1997).
[11] T. Nakamura *et al.*, Phys. Rev. Lett. **96**, 252502 (2006).
[12] T. Aumann and T. Nakamura, Phys. Scr. **2013**, 014012 (2013).
[13] A. M. Moro, K. Rusek, J. M. Arias, J. Gómez-Camacho, and M. Rodríguez-Gallardo, Phys. Rev. C **75**, 064607 (2007).
[14] A. M. Sánchez-Benítez *et al.*, Nucl. Phys. A **803**, 30 (2008).
[15] J. P. Fernández-García, M. Rodríguez-Gallardo, M. A. G. Alvarez, and A. M. Moro, Nucl. Phys. A **840**, 19 (2010).
[16] L. Acosta *et al.*, Phys. Rev. C **84**, 044604 (2011).
[17] A. Di Pietro *et al.*, Phys. Rev. C **69**, 044613 (2004).
[18] D. Escrig *et al.*, Nucl. Phys. A **792**, 2 (2007).
[19] J. P. Fernández-García, M. A. G. Alvarez, A. M. Moro, and M. Rodríguez-Gallardo, Phys. Lett. B **693**, 310 (2010).
[20] A. Di Pietro *et al.*, Phys. Rev. Lett. **105**, 022701 (2010).
[21] L. Acosta *et al.*, Eur. Phys. J. A **42**, 461 (2009).
[22] M. Cubero *et al.*, Phys. Rev. Lett. **109**, 262701 (2012).
[23] J. P. Fernández-García *et al.*, Phys. Rev. Lett. **110**, 142701 (2013).
[24] I. Tanihata, H. Savajols, and R. Kanungo, Prog. Part. and Nucl. Phys. **68**, 215 (2013).
[25] M. V. Andrés and J. Gómez-Camacho, Phys. Rev. Lett. **82**, 1387 (1999).
[26] R. Kanungo *et al.*, Phys. Rev. Lett. **114**, 192502 (2015).
[27] M. Cubero *et al.*, EPJ Web Conf. **17**, 16002 (2011).
[28] J. F. Ziegler, The Stopping and Range of Ions in Matter - SRIM, http://www.srim.org.
[29] M. Yahiro, N. Nakano, Y. Iseri, and M. Kamimura, Prog. Theor. Phys. **67**, 1467 (1982).
[30] N. Austern, Y. Iseri, M. Kamimura, M. Kawai, G. Rawitscher, and M. Yahiro, Phys. Rep. **154**, 125 (1987).
[31] Y. Sakuragi, Phys. Rev. C **35**, 2161 (1987).
[32] T. Matsumoto, T. Kamizato, K. Ogata, Y. Iseri, E. Hiyama, M. Kamimura, and M. Yahiro, Phys. Rev. C **68**, 064607 (2003).
[33] K. Rusek, N. Alamanos, N. Keeley, V. Lapoux, and A. Pakou, Phys. Rev. C **70**, 014603 (2004).
[34] C. Beck, N. Keeley, and A. Diaz-Torres, Phys. Rev. C **75**, 054605 (2007).
[35] J. A. Tostevin, F. M. Nunes, and I. J. Thompson, Phys. Rev. C **63**, 024617 (2001).
[36] D. J. Howell, J. A. Tostevin, and J. S. Al-Khalili, J. Phys.(London) **G31**, S1881 (2005).
[37] M. Rodríguez-Gallardo, J. M. Arias, J. Gómez-Camacho, A. M. Moro, I. J. Thompson, and J. A. Tostevin, Phys. Rev. C **80**, 051601(R) (2009).
[38] N. Keeley, K. W. Kemper, and K. Rusek, Phys. Rev. C **88**, 017602 (2013).
[39] L. C. Chamon, B. V. Carlson, L. R. Gasques, D. Pereira, C. De Conti, M. A. G. Alvarez, M. S. Hussein, M. A. Cândido Ribeiro, E. S. Rossi, and C. P. Silva, Phys. Rev. C **66**, 014610 (2002).
[40] A. J. Koning and J. P. Delaroche, Nucl. Phys. A **713**, 231 (2003).
[41] I. J. Thompson, Comput. Phys. Rep. **7**, 167 (1988).
[42] J. A. Tostevin (private communication).
[43] A. M. Moro, J. P. Fernández-García, M. A. G. Alvarez, and M. Rodríguez-Gallardo, EPJ Web Conf. **17**, 08001 (2011).
[44] P. N. de Faria *et al.*, Phys. Rev. C **82**, 034602 (2010).
[45] N. Austern and C. M. Vincent, Phys. Rev. C **23**, 1847 (1981).
[46] M. Y. M. Hassan, M. Y. H. Farag, E. H. Esmael, and H. M. Maridi, Phys. Rev. C **79**, 014612 (2009).
[47] I. J. Thompson and M. V. Zhukov, Phys. Rev. C **49**, 1904 (1994).
[48] F. Barranco, P. F. Bortignon, R. A. Broglia, G. Colò, and E. Vigezzi, Eur. Phys. J. A **11**, 385 (2001).
[49] G. Potel, F. Barranco, E. Vigezzi, and R. A. Broglia, Phys. Rev. Lett. **105**, 172502 (2010).
[50] T. Myo, Y. Kikuchi, K. Kato, H. Toki, and K. Ikeda, Prog. Theor. Phys. **119**, 561 (2008).
[51] H. Simon *et al.*, Phys. Rev. Lett. **83**, 496 (1999).